Effects of impurities on surface morphology: some examples

2009 J. Phys.: Condens. Matter 21 084215

(http://iopscience.iop.org/0953-8984/21/8/084215)

J. Phys.: Condens. Matter **21** (2009) 084215 (10pp) doi:10.1088/0953-8984/21/8/084215

Effects of impurities on surface morphology: some examples

Ajmi BH Hamouda[1,2,4], T J Stasevich[1,3], Alberto Pimpinelli[1,2] and T L Einstein[1]

[1] Department of Physics, University of Maryland, College Park, MD 20742-4111, USA
[2] LASMEA, UMR 6602, NRS/Université Blaise Pascal—Clermont 2, F-63177 Aubière cedex, France
[3] Fluorescence Imaging Facility, LRBGE, NCI, NIH, Bethesda, MD 20892, USA

E-mail: hammouda@umd.edu, stasevicht@mail.nih.gov, alpimpin@univ-bpclermont.fr and einstein@umd.edu

Received 22 August 2008, in final form 25 November 2008
Published 30 January 2009
Online at stacks.iop.org/JPhysCM/21/084215

Abstract
Small amounts of impurities are known to have remarkably great influence on surface morphology. We discuss three examples that arise in our research. First, we consider impurities codeposited during epitaxial growth, paying particular attention to Cu(100). After many layers of growth, the impurities can dramatically alter the surface morphology, changing the wavelength of the meandering instability and producing small square-base pyramids. Second, we consider the decoration of both island and vacancy island edges on Ag(111) with C_{60}. We use this system as a prototype to model how edge decoration with impurities can have a striking effect on the shape of the island as well as the dynamics of edge fluctuations. Finally, we show that about one per cent of pentacene quinone impurities alters the size of the critical nucleus in submonolayer pentacene deposition. This provides a platform on which to discuss our recent work characterizing the capture-zone distribution associated with the islands in terms of the generalized Wigner distribution, a simple one-parameter expression in which the characteristic exponent is the size of the smallest stable island.

(Some figures in this article are in colour only in the electronic version)

1. Introduction

Spurred on by experimental advances and technical importance, homoepitaxial growth has been a very active field over the last decade or two [1–4]. Theoretical interest, from a statistical mechanics perspective, has centered on the formulation of scaling laws, the computation of correlation functions, the investigation of islanding at submonolayer stages and possible roughening for thick overlayers, and identification of elemental units in growth. While most initial investigations assume pure homoepitaxy, frequent difficulties in establishing close correspondence between experimental systems and simple computational models has led investigators to consider the role of impurities. A recurrent issue is whether the impurities are clustered at the periphery or pervade the interior; the determining factor is typically the relative size of the attraction between the three possible pairs of impurity and host atoms. In either case, small concentrations of impurities can have dramatic effects on morphology.

In three separate cases, we[5] have encountered such phenomena. In the first, discussed in section 2, we consider how impurities affect growth and instabilities on Cu(100) [5, 6]. In this work, we take the impurities to be codeposited rather than predeposited before growth (so that the impurity atoms are well intermixed). We find that impurities alter the scaling exponent of the wavelength of the meandering instability versus deposition flux. We also find that impurities can produce small square-base pyramids observed in experiments and inexplicable in models not introducing impurities.

[4] Present address: Laboratoire de Physique Quantique, Faculté des Sciences de Monastir, Route de Kairouan, 5000 Monastir, Tunisia.

[5] In this paper, 'we' often means a subset of the authors plus some collaborators. This usage avoids the awkward but more accurate 'some of us (and other co-workers).'

In section 3, we consider a generic model of edge decoration of the step edges that form the boundary of adatom or vacancy islands [7]. The motivation was experiments in which single strands of C_{60} decorated the edges of such islands on Ag(111) [8, 9]. We show that the edge decoration can be used to engineer the shape of the islands. The impurities can also strikingly change the nature of the thermal fluctuations of the boundary of the islands.

In section 4, we discuss submonolayer growth, in particular the nature of the islands that form. Rather than the island-size distribution, we focus on the distribution of the areas of capture zones of the islands, the areas on the surface closest to each island (i.e., proximity or Voronoi cells). We have shown that the distribution of these areas has the form of the generalized Wigner distribution, a simple expression in which the single free parameter, a characteristic exponent, is the size of the smallest stable island [10]. We apply this idea to study the effect of impurity concentrations of order 1% in pentacene growth [11]. We find that the impurity significantly decreases the size of the smallest stable island. In this system, it is not *a priori* obvious where the impurities settle, but the evidence favors intermixing.

2. Effect of impurities on 2D nucleation and surface diffusion during epitaxial growth

2.1. Preliminaries

Recent progress in imaging techniques and better control of the growth methods, specifically molecular-beam epitaxy (MBE), allowed the fabrication of atomically smooth interfaces and has led to an increasing appreciation of the dramatic, detrimental, or beneficial effects that small amounts of impurities may have on the morphology of growing films. Adsorbates acting as *surfactants* can stabilize layer-by-layer growth of metal [12, 13] and semiconductor surfaces [14]. On the other hand, for the simple case of Pt(111) homoepitaxy, Kalff *et al* showed [15] that minute coverages of CO strongly increase the step-edge barriers for interlayer transport, thus enhancing three dimensional (3D) mound growth [16]. The effect of additional surface species on growth and nucleation also has obvious importance in more complex, technologically relevant deposition techniques such as chemical vapor deposition [17].

There is a fundamental theoretical distinction between homogeneous nucleation in a pure system and heterogeneous nucleation at defects or impurities. The increasing interest in such 2D nucleation, driven by the availability of atomic scale imaging techniques, has been primarily concerned with the former case [18]. However, defect nucleation plays an important role in many film systems, e.g. in the growth of metal clusters on alkali halides [19, 20]. Moreover, heterogeneous nucleation is at the heart of recently suggested methods for creating ordered nanostructure arrays by deposition on strain-relief patterns [21].

The effect of impurities on the island density and island decoration has been extensively studied both theoretically [3, 22, 23] and via kinetic Monte Carlo (KMC) simulations [24, 25]. Incorporated impurities were found to be of great importance for Cu self-annealing [26]. Cu(100) and surfaces vicinal to it are well suited for studies of MBE because they do not reconstruct. Experimental results show that during growth, the Cu(100) surface undergoes a mounding instability, and its vicinal surfaces experience meandering instability [27]. The meandering wavelength λ_m is found to scale with deposition rate F as $\lambda_m \sim F^{-\gamma}$ with an exponent $\gamma \approx 0.19$. When deposition is continued for at least 10 ML, small pyramids appear on the surface. The smaller value of the exponent γ rules out the Bales–Zangwill (BZ) instability (for which the expected value of the exponent is $\gamma = 0.5$) as a possible mechanism for the observed meandering instability. Other mechanisms, notably the kink Ehrlich–Schwoebel barrier effect (KESE) [28] and unhindered step-edge diffusion (USED) [29], do predict exponents closer to the observed value, but neither can explain the formation of small pyramids. Our primary goal is to account for these phenomena using the simplest model possible.

2.2. Description of the model

We studied the effect of impurities on epitaxial growth using KMC simulations of a two-species solid-on-solid (SOS) model of a simple cubic (rather than fcc) substrate [5]. That is, the impurities (i) are represented by a second particle species; they diffuse (diffusion barrier energy E_i^d) and interact attractively with the deposited adatoms (s) (bonding energy ϵ^{si}), but they do not attract each other ($\epsilon^{ii} = 0$) and hence do not nucleate impurity islands. The impurities are codeposited (rather than predeposited) during growth; they are shown to be responsible for quantitative and qualitative modification of the surface morphology. We also include an Ehrlich–Schwoebel barrier. More details of the model are given in [5].

In our minimal model, we assume no preferential adsorption of impurities at step edges; therefore, impurities do not decorate the island edge as they do in [3] and in the next section. We also neglect any barrier for crossing kinks along the step edge, since the KESE was unable to account adequately for the phenomena under scrutiny. Likewise, we do not include preferential diffusion along the step edge, since USED mechanism also could not explain the experiments fully. While both aspects are doubtless important for a full treatment of the system, our goal, again, is to find the *simplest* model that reproduces the observed behavior. We consider both mobile and immobile impurities. While they produce significantly different behavior, both cases exhibit strong dependence of the island density on the flux and concentration of impurities. In particular, codeposited impurities seems to be the most likely candidate to explain the main features of the morphological details for Cu (1 1 17); no other proposed mechanism can meet this test.

2.3. Submonolayer regime: island density and diffusion length

In the absence of impurities, the scaling relation between island density N, deposition flux F, and the adatom diffusion coefficient D has been well established theoretically, numerically, and experimentally [3]:

$$N \sim (F/D)^{\chi}. \tag{1}$$

The exponent χ can be derived from a rate-equation analysis [30] expressed in terms of the size i^* of the largest

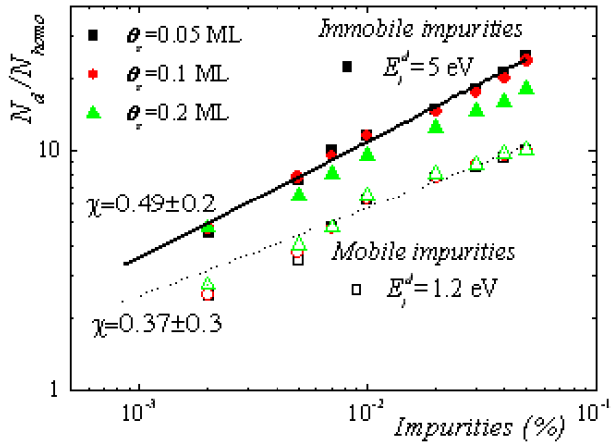

Figure 1. Relative increase of island density N/N_{homo} as a function of the concentration of codeposited impurities θ_i for mobile, $E_i^{\text{d}} = 1.2$ eV (open symbols) and immobile, $E_i^{\text{d}} = 5$ eV (filled symbols) impurities and three values of the coverage: $\theta_s = 0.05$ ML (squares), $\theta_s = 0.1$ ML (circles), $\theta_s = 0.2$ ML (triangles). The flux is $F = 0.001$ ML s^{-1}, and temperature $T = 500$ K, as in figure 1 of [22]. Lines are fits with equation (3).

unstable cluster (the 'critical nucleus'):

$$\chi = i^*/(i^* + 2). \tag{2}$$

Attractive impurities alter equation (1) in several ways [3]. First, impurities may act as nucleation centers, thus effectively decreasing i^* and therefore χ; in the extreme case of immobile adatom traps, the limit of spontaneous nucleation with $i^* = \chi = 0$ would be realized. Second, impurities decorating island edges may induce energy barriers to attachment. Kandel [31] showed that, provided these barriers are sufficiently strong, the exponent χ in equation (1) is increased such that equation (2) is replaced by $\chi = 2i^*/(i^* + 3)$. Both mechanisms imply an increase of the island density compared to the case of pure homoepitaxy. Third, impurities could facilitate the breakup of small clusters, thus effectively increasing i^* and decreasing the island density. In figure 1 we show the enhancement factor N/N_{homo} as a function of impurity coverage at fixed flux $F = 0.001$ ML s^{-1}, in good agreement with figure 3 in [22]. This factor is predicted to be [22]:

$$N/N_{\text{homo}} \approx [1 + \theta_i\{\exp(\epsilon^{si}/k_{\text{B}}T) - 1\}]^{\chi} \tag{3}$$

where θ_i is the impurity concentration. For mobile impurities $\chi = 0.37 \pm 0.3$. For immobile impurities, a similar fit leads to $\chi = 0.49 \pm 0.2$, which is close to the actual value of the island density scaling exponent measured for homoepitaxy [5]. At larger θ_i the data for immobile impurities show significant dependence on the island density at adatom coverage θ_s, similar to the behavior observed in [3] for predeposited mobile impurities at high flux. Moreover, equation (3) shows that for a given coverage, this ratio is very sensitive to a small variation of bond energy ϵ^{si} between the host and impurity species. Hence, it should be a theoretically possible (though not straightforward experimentally) to tune the island density by adjusting the strength of this attraction.

Finally, figure 1 shows that mobile impurities are much less effective in increasing the island density than immobile defects. Since the microscopic processes of deposition, diffusion, capture at impurities, and detachment from impurities do not significantly depend on the impurity mobility, the different behavior can be attributed to the depletion of mobile impurities due to their capture at existing islands [3, 22]. A quantitative treatment of this effect requires an analysis of rate equations for the different surface species [20].

Our results agree with earlier work by Kotrla *et al* [22], who investigated the influence of mobile and immobile impurities on island nucleation. Our figure 1 agrees completely with figure 3 of [22]. It shows that slowly diffusing impurities (closed symbols), even though at very low coverage, change considerably the dependence of the island density, and thus of the adatom diffusion length, on the deposition rate. Note that in [22] impurities are predeposited on the substrate, while they are codeposited in our model. In both cases, the effective adatom diffusion length is essentially independent of the deposition rate when the impurities are immobile. Since this diffusion length sets the scale for the unstable wavelength the BZ instability, impurities will likely alter the characteristics of the meandering instability as a function of the deposition rate.

2.4. Multilayer regime

For at least 10 ML deposition, a small concentration of codeposited impurities has a dramatic effect on the meandering wavelength and the surface morphology. (Unless they are surfactants, predeposited impurities will be buried by this stage.) For growth on a pure system (one species model), the simulated surface (figure 2(a)) shows the meandering instability characterized by smooth fingers separated by deep grooves. Quantitatively, the meandering wavelength agrees with the $\lambda_{\text{m}} \sim F^{-1/2}$ prediction of BZ linear theory. However, when a second species is included, small rhombus-based pyramids on (0 2 24) or square-based pyramids on (1 1 17) start to appear (see figures 2(b) and (c)) after a few monolayers. These pyramids are strikingly monodisperse in shape and size (their size distribution being narrower than that of similar pyramids formed on high-symmetry (001) surfaces). Their surface density (but not their size) seems to increase with both time and deposition rate, but their size and shape are insensitive [5]. Their linear size is essentially the same as the width of the 'finger' on top of which they form. These square-based pyramids have been interpreted as the result of a secondary mounding instability that is observed to follow meandering in simulations [32]. However, the secondary mounding instability leads in general to large mounds, whose size is not directly related to the meandering instability [6]. Furthermore, simulations show that such mounds tend to disrupt the meander structure and to completely cover the surface, making it eventually impossible to distinguish a mounded vicinal from a mounded high-symmetry surface. This is very different from what is depicted in figure 2(c).

Besides the appearance of square-shaped pyramids induced by impurities, we discovered that the meandering

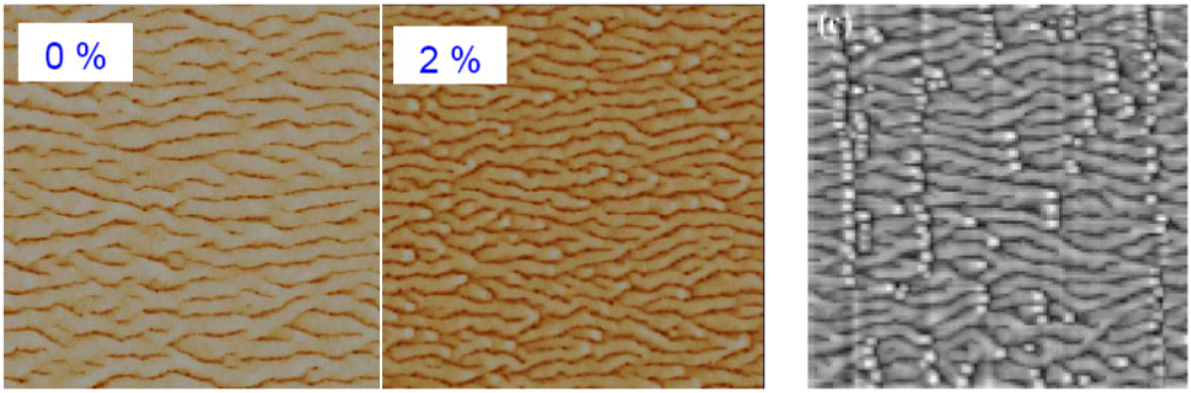

Figure 2. Experimental [27] (right panel) and the simulated close-packed step surfaces for pure Cu deposition (left panel) and deposition with 2% impurities (middle panel), at $T = 285$ K, as in the experimental images shown in figure 3 of [27b]. For the pure case, $\epsilon^{ss} = 0.13$ eV and $E_s^{\mathrm{d}} = 0.4$ eV. The hopping barrier for impurities is $E_i^{\mathrm{d}} = 0.6$ eV, and the adatom–impurity binding energy is $\epsilon^{si} = 0.2$ eV. The simulations (for 20 ML deposition) produce morphologies indistinguishable from the experimental picture. Close inspection of the experimental micrograph shows that the pyramids tend to align along the step direction, a feature missing in the simulations. Elastic interactions or a slightly varying average step density, both obviously absent in the simulations, may explain the discrepancy.

wavelength shortens; this decrease is clearly visible in figure 2(b) (with 2% impurities) compared to figure 2(a) (pure) [5]. This finding leads to a physical explanation for the disagreement between theory and experiment in the λ_{m} versus $F^{-\gamma}$ behavior, as discussed in [5].

In our KMC simulations the impurities must satisfy the following two conditions in order to reproduce the exact λ_{m} versus F scaling behavior and the formation of small pyramids: (i) the bond energy ϵ^{si} between an impurity atom and a Cu adatom must be stronger than the Cu–Cu bond ϵ^{ss}, and (ii) the impurities must diffuse less rapidly than the Cu adatoms ($E_i^{\mathrm{d}} > E_s^{\mathrm{d}}$). Due to their stronger bonds with Cu adatoms, we expect that impurity atoms slow down Cu-adatom diffusion, thereby shortening the diffusion length and making λ_{m} less sensitive to deposition rate (F). Also, impurity atoms act as nucleation centers for the formation of small pyramids. Though several common elemental impurities (such as H, C, and O) are likely to contaminate Cu films [33], the exact type of impurity responsible for the observed instabilities cannot be deduced from KMC simulations alone. Doing that requires a systematic evaluation of surface energies and barriers for all likely impurity atoms. Our preliminary calculations [34] using density functional theory (DFT) show that none of these impurities lead to energies satisfying our two criteria. (Furthermore, such impurities would likely cluster together [35].) However, we find that mid-transition elements to the left of Cu in the periodic table, such as Fe and Mn, do fulfil our requirements. Such elements are likely to come from source from which the Cu is evaporated [35]. However, it is unlikely that there is sufficient (i.e., several per cent) concentration of such mid-transition metals to create the observed effects. A third possibility is CO, which in low concentrations also seems to have suitable bond and barrier energies [36]. However, it is not clear whether CO impurities would become buried during growth.

There are several directions that future investigations might take [6]. Predeposited impurities can decorate island edges during growth, given some suitable choice of binding between impurities and adatoms [3]. Then it is straightforward to extract some general rules about the kinetics of adsorbates. However, when impurities are codeposited, the detailed atomistic kinetics and energetics of the interaction between adsorbate and deposited material influence the growth mode, therefore confounding the formulation of general rules. E.g., edge decoration is no longer favored when impurities are codeposited. Instead, such impurities are more likely to be trapped inside the islands, affecting the diffusion length of the deposited material. Impurities with lower mobility and binding energy than those of majority-element adatoms act as traps that affect the growth process by serving essentially as nucleation centers, slowing down the surface diffusion and diminish the anisotropy near step edges; similar effects are expected at lower temperatures corresponding to the growth experiments. Thus, as is shown in our KMC simulations (figure 3), a vicinal surface which is unstable to step-bunching can be stabilized by including a small concentration of impurities [6]. Weeks and co-workers [37, 38] have modeled the dramatic effects that impurities can have on step evolution.

3. A model for impurity step decoration: C_{60}/Ag(111)

Steps on crystalline surfaces can be energetically favorable anchor points for impurities. Whereas steps play a vital role in shaping the evolution of surfaces, they constitute an insignificant fraction of the surface area. It therefore only requires a small amount of impurities to fully decorate surface steps and dramatically change surface properties. Although this extreme sensitivity to impurity concentration can be troublesome for controlling surface growth, in reverse the sensitivity can be exploited to produce promising surfaces structures, including evenly spaced molecular chains [39], tunable metal–nanoparticle gaps [40], and uniform arrays of quantum dots [41].

Often impurities are too small to be seen by STM, so their presence can only be discovered indirectly through their

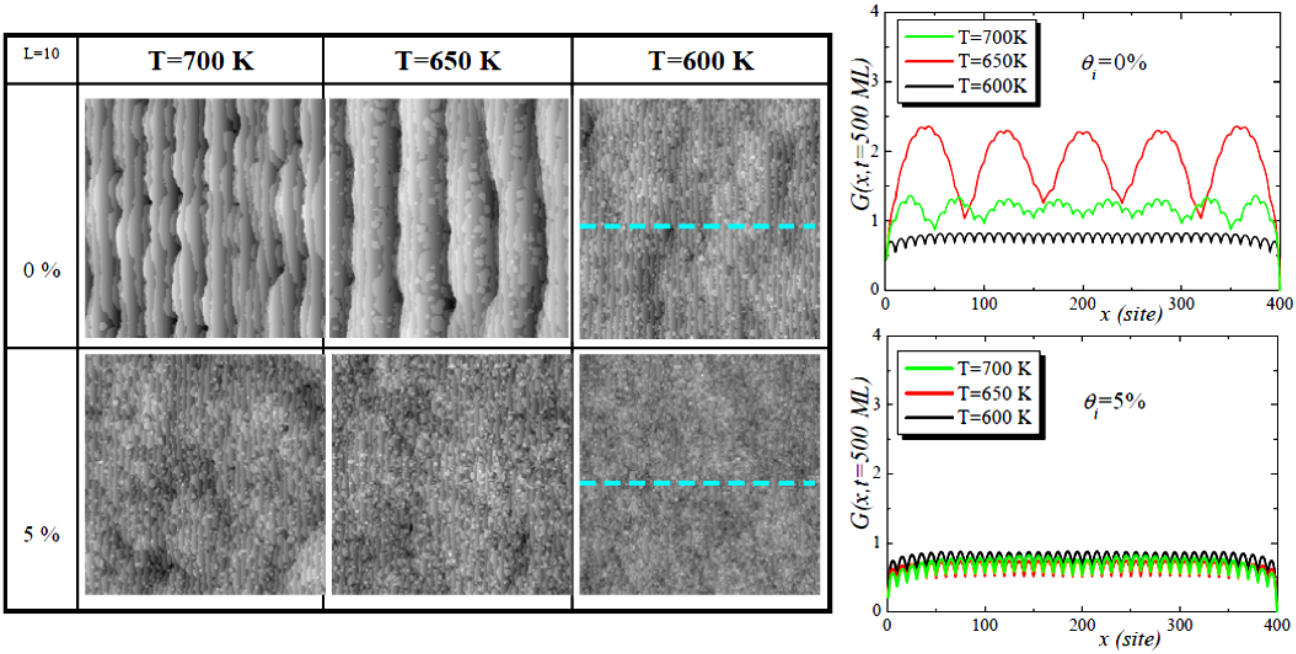

Figure 3. Effect of temperature and of impurities on the step-bunching instability. Simulated morphological evolution for: clean surface (top panel) and with impurities (5%, bottom panel). Parameters: (400 × 400) lattice with periodic boundary conditions, mean step spacing $L = 10$, $F = 0.5$ ML s^{-1}, thickness = 500 ML, $E_s^{\rm d} = 1.0$ eV, $E_i^{\rm d} = 1.2$ eV, $\epsilon^{ss} = 0.3$ eV, $\epsilon^{si} = 2\epsilon^{ss}$, $\epsilon^{ii} = 0$ eV, $E_{iES} = 0.1$ eV. The height–height correlation function $G(x)$ is plotted for separations along the downstairs direction $\hat{x}$, as indicated by the teal horizontal dashed line in the third column of lattice images. The heights are relative to the vicinal plane rather than the terrace plane.

effects. This can lead to confusion. For example, Pt(111) adatom islands were observed to dramatically rotate by 60° as the temperature increased. Initially this was reported as the temperature-dependent evolution of the equilibrium island shape, which many struggled to reconcile with theory [42]. Only later was it realized that the effect was actually due to impurities, in this case the concentration of CO on the surface [15]. Apparently just 10^{-3} ML of CO was enough to fully decorate the island step edges and produce the dramatic shape change. When the temperature rose, the CO evaporated and the islands reverted back to their equilibrium shapes. As this example illustrates, trace impurities are enough to produce remarkable and sometimes mysterious morphological changes in stepped structures.

To better understand how step decoration by relatively small amounts of impurities can produce significant changes in surface properties, we have studied the adsorption of C_{60} on Ag(111) [8, 9]. This system is ideal for two reasons: First, C_{60} is a relatively large spherically-symmetric model impurity that is easy to distinguish from Ag step atoms via STM, so the geometry of step decoration can be directly measured and analyzed. Second, C_{60} remains mobile on Ag(111) at room temperature, so C_{60} decorated stepped structures equilibrate and continue to dynamically fluctuate.

When C_{60} molecules are deposited on Ag(111) at 300 K, they rapidly attach to the lower edges of Ag steps, but continue to diffuse along these steps (figure 4(a)). If the step is part of a larger hexagonal Ag equilibrium adatom or vacancy island, the C_{60} can diffuse along the entire island perimeter, though they tend to nucleate and form single-layer chains near the island corners. As the chains lengthen, the corners round until the chains ultimately meet one another and link to form a single-stranded C_{60} 'necklace' that fully decorates the island step-edge perimeter, now circular in shape. Once the necklace is complete, rather than forming a thicker double-stranded necklace, additional C_{60} conglomerates to form 'ears' near the corners of the original undecorated island. By carefully controlling the C_{60} coverage, islands decorated by just a single-layer C_{60} necklace can be generated (figure 4(b)).

To describe these observations analytically requires at least three key binding energies: $\epsilon^{\rm AA} \approx 0.234$ eV between two nearest-neighbor Ag adatoms (deduced from fits to the orientation dependence of the step free energy on Ag(111) [43] and analogous to ϵ^{ss} in the previous section), $\epsilon^{\rm AC}$ between a C_{60} molecule and the close-packed Ag step edge (analogous to ϵ^{si}), and $\epsilon^{\rm CC}$ between two nearest-neighbor C_{60} molecules (analogous to ϵ^{ii}). As discussed in the opening paragraphs of this section, it is again the relative strengths of these basic bonds that controls how C_{60} interacts with the surface steps. If the attraction to Ag is too strong, the C_{60} could penetrate steps to maximize its contact with Ag adatoms. Alternatively, if the attraction is too weak, the C_{60} could prefer to bunch rather than fully decorate the step. Since decoration is complete and necklaces form, the strength of $\epsilon^{\rm AC}$ should fall between the other two bond energies, that is, $\epsilon^{\rm AA} > \epsilon^{\rm AC} > \epsilon^{\rm CC}$, in contrast to the inequalities implicit in the previous section.

Decoration by C_{60} molecules alters both the equilibrium and dynamic properties of the Ag steps. Remarkably, decorated islands continue to fluctuate with a magnitude similar to undecorated islands, but at a frequency (∼1 Hz) two orders of magnitude slower [9]. Moreover, decorated islands are stabilized by the C_{60} necklace, i.e. they decay at a slower

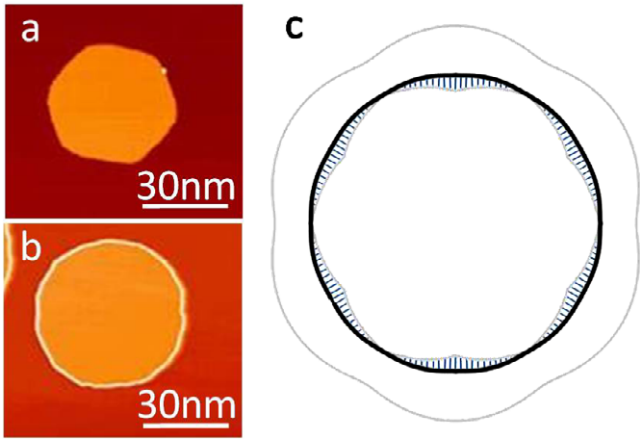

Figure 4. (a) Deposited C_{60} (beige dot just below the upper right corner) initially decorates the corner of a hexagonal Ag(111) adatom island (light gray (orange online) on darker gray (darker orange online) substrate). (b) C_{60} coverage is tuned so an adatom island becomes fully decorated by a single-layer C_{60} necklace. This causes its equilibrium shape to become circular. (c) The free energy of undecorated islands (outer gray curve with fully-kinked direction vertical) corresponds to a hexagonal equilibrium island shape, as shown in (a). Upon decoration, the free energy is lowered and becomes circular (black curve), corresponding to the observed circular islands. This is due to an orientation-dependent energy gain (region between inner and outer gray curves) that favors fully-kinked directions and an orientation-dependent entropy cost (striped region) that favors high-symmetry, unkinked directions. These partially cancel to produce an orientation-independent circular free energy (black curve).

rate than undecorated islands. In essence, the C_{60} necklace acts like a kinetic barrier that prevents Ag step-edge adatoms from detaching. However, C_{60} does not appear to significantly alter the diffusion of Ag atoms *along* the step edge. In an earlier paper [8], we showed that bare Ag steps bound by C_{60} molecules at both ends continue to fluctuate with step-edge diffusive kinetics, as though the C_{60} were not even there, regardless of the length of the bare portion of the step. In short, C_{60} neither pins steps nor prevents the flow of adatoms along the step edge, but it does diminish the rate of step-edge adatom detachment.

Besides analyzing the fluctuations of bare Ag(111) steps bound by C_{60} molecules, we also analyzed the step-edge fluctuations of relatively small islands fully decorated by single-layer necklaces containing on the order of 100 C_{60} molecules [9]. To adequately sample the fluctuations, we analyzed multiple data sets consisting of sequential STM images of single islands (figure 4(b) shows a sample frame). The largest set contained 600 frames with temporal resolution 13.1 s for a total acquisition time of 130 min. From each frame, we digitized the decorated island edge and averaged the results together to verify the equilibrium island shape $R(\theta) = R$ is circular, where θ is the angle measured from the Ag adatom high-symmetry direction. We then subtracted the equilibrium shape from each digitized island edge to quantify the island fluctuations $r(\theta)$ about that shape.

According to the Langevin analysis, when the fluctuations $r(\theta)$ are decomposed into their component Fourier modes $r_k(\theta)$, k being the wavenumber, each mode shares $k_B T/2$ of thermal energy. This provides an energy scale from which the absolute decorated step-edge stiffness $\tilde{\beta}(\theta)$ can be calculated. Specifically, the correlations $G_k(t)$ of each mode are expected to decay as [44, 45]

$$G_k(t) = \langle [r_k(t+t_0) - r_k(t_0)]^2 \rangle = \frac{k_B T}{\pi \tilde{\beta} k^2}(1 - e^{-t/\tau_k}) \quad (4)$$

where the prefactor is the mean-squared amplitude of the radial fluctuations in the kth mode and τ_k the time constant for that mode. Fits of the prefactor for the first $k = 1$–12 modes confirm the inverse-squared power-law dependence, from which we determined $\tilde{\beta} \approx 0.65$ eV nm^{-1} [9]. This is similar to that of bare steps where $\tilde{\beta} \approx 0.67$ eV nm^{-1} [8, 43], as expected qualitatively based on the amplitude of the fluctuations. Interestingly, fits reveal $\tau_k \propto k^{-2}$, as would be expected for attachment-detachment kinetics. This is in stark contrast to the correlated fluctuations of bare Ag steps, where $\tau_k \propto k^{-4}$, indicative of conserved step-edge diffusive kinetics. Mysteriously, then, although the C_{60} are clearly attracted to the bare Ag steps, they fluctuate with distinctly different kinetics after decoration.

The origin of the distinct fluctuations can be gleaned from repeated STM line scans over the center of a single C_{60} molecule decorating a step. These reveal the C_{60} periodically 'hops' a single Ag lattice constant toward the step and then quickly returns, apparently preferring to be further than closer [9]. Evidence for these hops also appears in the analysis of fluctuating islands, which reveal neighboring trios of C_{60} molecules form preferred angles, the smallest of which is 15°, as would be expected if one of the C_{60} were to hop towards the step by a single Ag lattice constant. Together, this data suggests the non-conserved hops, which are only weakly coupled to the underlying step, are responsible for the distinct attachment-detachment like kinetic fluctuations.

We conclude our discussion of C_{60} decoration of Ag steps by returning to perhaps its most striking feature, the island shape change. Once a bare step is decorated, its stiffness and line tension are lowered, as the fluctuation analysis has shown. For shape change, though, the line tension must be anisotropically lowered. Evidence for this anisotropy can be seen in necklace formation, where C_{60} chains grow out from the island corners. This occurs because corners have more Ag kinks. These kinks can rearrange themselves into double kinks that are in registry with nearest-neighbor C_{60} (separation 1 nm), thereby creating a bond that geometrically should be twice as strong ($2\,\epsilon^{AC}$) as those along high-symmetry steps lacking kinks. Thus, the energy of fully-kinked steps is lowered more than steps along other directions when decorated, imparting an orientation-dependent C_{60} attachment energy that favors fully-kinked steps.

Besides energy, entropy also plays a key role in altering the anisotropy of the decorated step line tension. When C_{60} molecules attach to the step edge, the step pays an entropy penalty. Of all possible orientations, fully-kinked steps pay the highest penalty because these have the most kinks and therefore the highest initial entropy. (See [43, 46] for a detailed

discussion of this 'bare' entropy.) After decoration, however, these step rearrange into a single optimal configuration with minimal entropy: double kinks form that are in registry with neighboring C_{60} to maximize molecular contact. On the other hand, high-symmetry close-packed steps have no kinks, so both their initial and final entropy is minimal, meaning the entropy cost of decoration is also minimal. In essence, although fully-kinked steps gain the most energetically from decoration, they also pay the highest entropy cost. In this case, the two effects partially cancel to yield a circular decorated island shape, as shown in figure 4(c).

Using this type of analysis, the circular islands can reveal even more about the key bond energies: ϵ^{AA}, ϵ^{AC}, and ϵ^{CC}. Just as the general decoration morphology depended sensitively on these energies, so too does the decorated island shape. If ϵ^{AC} is very strong, the energy benefit gained by fully-kinked steps upon decoration would dominate, so we would expect these steps to appear more prominently in the equilibrium islands. Were this the case, the originally hexagonal Ag islands would rotate by 30° when decorated (that is, fully-kinked steps would become more favorable than unkinked). On the other hand, if ϵ^{AC} is weak compared to ϵ^{AA}, the island shape would not dramatically change (unkinked steps would still be most favorable). We have recently quantified this dependence together with entropic effects and combined it with our earlier measurement of the absolute line tension to fit the three binding energies to the circular island shape [7]. Our analysis reveals $\epsilon^{AC} \approx 0.13$ eV and $\epsilon^{CC} \approx 0.03$ eV. As expected, these are consistent with the hierarchy of energy required for step decoration to occur.

In short, C_{60}/Ag(111) provides an ideal system to study how just a few impurities can decorate steps to dramatically change both the equilibrium and dynamic properties of surface stepped structures. The ability to visualize C_{60} decoration provides compelling evidence for anisotropic attachment energies, and the dynamic fluctuation analysis allows for a more quantitative analysis of entropic effects. In general, we expect both the energy and entropy of decoration to contribute to island shape change, with fully-kinked steps becoming more favorable energetically, but paying the largest entropy penalty. Depending on the relative strengths of these two effects, decorated islands are expected to either round or rotate, similar to the morphologies discussed at the outset.

4. Capture-zone distributions

Another way the impurities impact growth is seen in the morphology at submonolayer coverages. It has long been popular to investigate this regime in terms of distributions of island sizes. Over a decade ago Mulheran and Blackman [47] pointed out that it may be more fruitful to study instead the capture zones of these islands. These capture zones are essentially proximity or Voronoi (generalized Wigner–Seitz) cells constructed with respect to the centers of the islands. In particular, the capture-zone distribution (CZD) can be well described in terms of a single-parameter distribution. We have found that this characteristic power-law exponent is just the size of the smallest stable island, conventionally denoted i^*+1, where i^* is the 'critical nucleus' size discussed in section 2, and therefore i^*+1 the size of the smallest stable cluster. We find that less than a per cent of impurities can significantly decrease this exponent, and so the value of i^*.

Our approach uses the generalized Wigner distribution (or surmise), which, as we capsulize, describes the distribution of a fluctuating quantity. The fundamental axiom underlying the application of random matrix theory to these problems is Wigner's insightful expectation that systems governed by different Hamiltonians but having some common symmetry ought to exhibit some generic properties, analogous to statistical mechanics considering ensembles of systems with the same Hamiltonians but different initial conditions [48, 49]. The three generic symmetries of Hamiltonians are orthogonal, unitary, and symplectic (corresponding to time-reversal invariant with rotational symmetry, time-reversal invariant, and time-reversal invariant with half-integer spin and broken rotational symmetry, respectively). Formulated to describe the spacings between energy levels in nuclei, the theory is useless for average quantities but finds that the fluctuations of large numbers of levels becomes independent of the particulars of the level spectra and the weighting factors (typically Gaussian or circular) and attains a universal form. Wigner surmised that the distribution of spacings for this limit could be described by that of the opposite limit of just two levels, which can readily be shown [50] to have the form

$$P_\varrho(s) = a_\varrho s^\varrho \mathrm{e}^{-b_\varrho s^2}$$
$$a_\varrho = \frac{2\left[\Gamma\left(\frac{\varrho+2}{2}\right)\right]^{\varrho+1}}{\left[\Gamma\left(\frac{\varrho+1}{2}\right)\right]^{\varrho+2}} \qquad b_\varrho = \left[\frac{\Gamma\left(\frac{\varrho+2}{2}\right)}{\Gamma\left(\frac{\varrho+1}{2}\right)}\right]^2 \tag{5}$$

where $\varrho = 1$, 2, and 4, respectively, for the 3 symmetry classes and s is the fluctuating variable divided by its mean. While equation (5) is not exact, this simple expression is nonetheless an excellent approximation [51].

Over the last decade, we have devoted much attention to applications of these ideas to problems in surface science, first to terrace-width distribution (TWD) on vicinal surfaces (i.e., the distance between adjacent steps on a surface misoriented from a facet direction),[6] and more recently to capture-zone distributions of islands in submonolayer growth. Ultimately, these problems can be related to Dyson's 1D Coulomb gas model [53] and his model for interacting Brownian particles [48, 51, 54, 55], and the exponent ϱ to the strength

[6] One views step configurations as the worldlines in one dimension (1D) of particles, spinless fermions since the steps cannot cross. These fermions repel each other, a translation of the A/w^2 elastic repulsion between steps separated by w. Accordingly, the Calogero–Sutherland model [52] describes the problem. In the thermodynamic limit the ground-state many-particle wavefunction squared, giving the spacing distribution, is related to Dyson's 1D Coulomb gas model [53] and his model for interacting Brownian particles [48, 51, 54, 55]. Consequently, equation (5) should describe excellently the TWD for the special cases $\varrho = 1$, 2, and 4, where the dimensionless combination $\tilde{A} \equiv A\tilde{\beta}/(k_\mathrm{B}T)^2 = \varrho(\varrho-2)/4$. In both numerical tests and in fits to experimental data, we have found that a 'generalized Wigner distribution', namely equation (5) taken for arbitrary $\varrho \geqslant 2$ (and so $\tilde{A} > 0$), provides an optimal description of the TWD and that the extracted values of ϱ from the experimental fits can be as large as about 10. See reviews [56–58] for details.

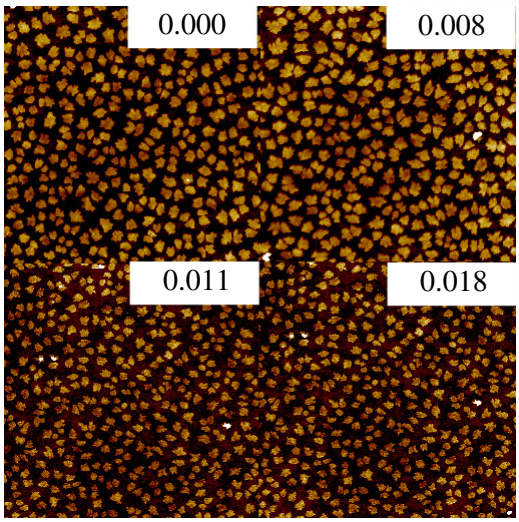

Figure 5. AFM images (10 μm × 10 μm) at 0.3 ML Pn/PnQ on SiO_2 with 0%, 0.008%, 0.011%, and 0.018% PnQ (by number, not mass). Similar to, but different images from, figure 1 of [11]. (Figure courtesy of B R Conrad and E D Williams.)

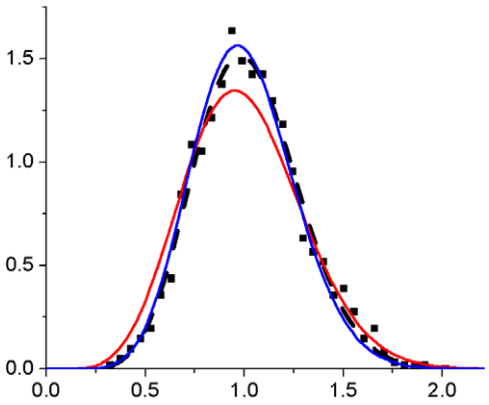

Figure 6. Probability distribution function of capture-zone areas versus s, the capture-zone area divided by its average value. The data points, indicated by small squares, are for pure Pn and (lower panel) for 0.011 number-fraction PnQ. In each panel the red (wider) curve is the generalized Wigner distribution $P_\varrho(s)$ given in equation (5), for $\varrho = 5$, while the blue (narrower) curve is for $\varrho = 7$. The thick black dashed line gives the best fit to the data using equation (5). See text for further discussion. (Figure courtesy of B R Conrad and E D Williams.)

of the repulsion between particles. Our strategy has been to use equation (5) for general values of ϱ rather that just the three special cases, and to focus on physical properties that can be extracted from the fitted value of this exponent. We note that the general feature underlying all the applications of equation (5) rely on some long range repulsion that suppresses small s and some force at the other extreme that militates against very large values of s. For CZDs, s is the CZ area divided by the mean of these areas. When a new island nucleates, its initial size is miniscule, but its CZ is comparable in size to others in its neighborhood. At the other extreme, large CZ areas are suppressed by an effective force from the other CZs.

Since there is no symmetry argument underlying equation (5) for non-special ϱ, we have sought other supporting arguments [59]. Recently two of us have developed a 1D Fokker–Planck description of the evolution of the TWD[7], which we have extended to deal with CZs in submonolayer growth [10]. As we have argued in detail elsewhere [60, 61],

$$\frac{\partial P(s,\tilde{t})}{\partial \tilde{t}} = \frac{\partial}{\partial s}\left[\left(2b_\varrho s - \frac{\varrho}{s}\right)P(s,\tilde{t})\right] + \frac{\partial^2}{\partial s^2}[P(s,\tilde{t})], \quad (6)$$

where the dimensionless time $\tilde{t}$ is the actual time divided by a characteristic decay time. The steady-state solution of equation (6) is easily seen to be $P_\varrho(s)$.

The stochastic aspect of the problem is that a newly deposited atom on a surface need not necessarily attach to the island nearest it: not all atoms landing in the capture zone attach to the island determining the CZ. We have shown that the capture-zone distribution (CZD) is generally well described by equation (5), with the exponent ϱ identified (in 2D) as $i^* + 1$. This relation provides a good accounting of both experimental CZDs and those generated by kinetic Monte Carlo simulations by various groups (though with some problems when the point-island approximation for islands is used). Again there is an argument for the evolution of the CZD based on equation (6); see [10].

We apply this formalism to pure and impure submonolayer pentacene (Pn) films on SiO_2, as described in detail in [11]. Figure 5 gives atomic force microscope (AFM) images for a pure film at 0.3 monolayers (ML) coverage and for three different number concentrations of pentacene quinone (PnQ) impurities, of order 1%. There is a qualitative difference between the two upper panels (pure and <1% PnQ) (as well as a similar image at 0.006% in figure 1 of [11]) and the two lower panels at higher PnQ concentration. The islands in the latter are smaller; quantitative analysis shows that the average area decrease by about a factor of 4. We will find that their normalized distribution tends to be broader.

To analyze the CZD of these images, Conrad *et al* [11] identify the centers of each island and construct from them the associated Voronoi polygons (cf figure 3 of [11]). As shown in figure 6, the pure case is well described by $P_7(s)$; the deduced best fit is obtained for $\varrho = 6.8 \pm 0.4$, depicted by the thick dashed curve barely visible under the curve for $\varrho = 7$. Once there is about 1% PnQ, the value of ϱ decreases by about 2. For the illustrated case of 0.011 number-fraction PnQ, the deduced best fit is $\varrho = 5.3 \pm 0.2$ and remains so to the highest impurity fraction examined (5.2% PnQ). Thus, PnQ impurities are linked to a decrease in the critical nucleus size from ∼6 to ∼4; i.e., the smallest stable cluster decreases from ∼7 to ∼5. Remarkably, the island-size distribution is largely unaffected by the PnQ. It can be described by a Wigner distribution with $\varrho \approx 4$ for all the studied percentages of PnQ. The observation that ϱ is smaller for the ISD than the CZD is consistent with other studies. Both Monte Carlo simulations and experiments, in particular those on pure Pn [62], have shown that the CZD is less sensitive to D/F than the ISD.

[7] We start from Dyson's Coulomb gas model [53] and make a mean-field-like approximation that focuses on a single separation w and assumes that all the particles—other than the two bounding w, are at their equilibrium positions.

As discussed in [11], the dependence of critical nucleus size on impurity concentration could be well be due to a preferential attraction between Pn and PnQ molecules, stabilizing smaller clusters. In this case, the PnQ is likely to be incorporated in the interior of grains, like impurities on Cu (discussed in section 2), rather than at the edge, as for C_{60} on Ag(111) (discussed in section 3). There is also information from transport measurements consistent with internal rather than exclusively edge-bound PnQ.

Acknowledgments

Work at U. of Maryland was supported by the NSF-MRSEC, Grant DMR 05-20471, with ancillary support from the Center for Nanophysics and Advanced Materials (CNAM) and DOE CMSN grant DEFG0205ER46227. We benefited greatly from our interactions with Ellen D Williams, John D Weeks, and Raymond J Phaneuf, and their groups, especially Brad Conrad and Chenggang Tao, and with Rajesh Sathiyanarayanan. ABHH and AP thank P E Hoggan and the late H-J Ernst for helpful exchanges. We are particularly grateful to B R Conrad and E D Williams for permission to use two unpublished figures from his dissertation research.

References

[1] Pimpinelli A and Villain J 1989 *Physics of Crystal Growth* (Cambridge: Cambridge University Press)
[2] Saito Y 1996 *Statistical Physics of Crystal Growth* (Singapore: World Scientific)
[3] Kotrla M, Krug J and Šmilauer P 2000 *Phys. Rev.* B **62** 2889 and references therein
[4] Michely T and Krug J 2004 *Islands, Mounds and Atoms* (Berlin: Springer)
[5] Ben-Hamouda A, Absi N, Hoggan P E and Pimpinelli A 2008 *Phys. Rev.* B **77** 245430
[6] BH Hamouda A 2007 Morphologie et stabilité des surfaces cristallines nanostructurées, dynamique des instabilités: théorie et modélisation *PhD Dissertation* Université Blaise Pascal—Clermont 2, Doctoral School of Fundamental Science No 531, unpublished
[7] Stasevich T J, Tao C, Cullen W G, Williams E D and Einstein T L 2009 *Phys. Rev. Lett.* submitted
[8] Tao C, Stasevich T J, Einstein T L and Williams E D 2006 *Phys. Rev.* B **73** 125436
[9] Tao C, Stasevich T J, Cullen W G, Einstein T L and Williams E D 2007 *Nano Lett.* **7** 1495
[10] Pimpinelli A and Einstein T L 2007 *Phys. Rev. Lett.* **99** 226102
[11] Conrad B R, Gomar-Nadal E, Cullen W G, Pimpinelli A, Einstein T L and Williams E D 2008 *Phys. Rev.* B **77** 205328
[12] van der Vegt H A, Thornton J M C, van Pinxteren H M, Lohmeier M and Vlieg E 1992 *Phys. Rev. Lett.* **68** 3335
[13] Meyer J A, van der Vegt H A, Vrijmoeth J, Vlieg E and Behm R J 1996 *Surf. Sci.* **355** L375
[14] Voigtländer B, Zinner A, Weber T and Bonzel H P 1995 *Phys. Rev.* B **51** 7583
[15] Kalff M, Comsa G and Michely T 1998 *Phys. Rev. Lett.* **81** 1255
[16] Kalff M, Šmilauer P, Comsa G and Michely T 1999 *Surf. Sci. Lett.* **426** L447
[17] Andersohn L, Berke T, Kóhler U and Voigtländer B 1996 *J. Vac. Sci. Technol.* A **14** 312
[18] Brune H 1998 *Surf. Sci. Rep.* **31** 121
[19] Hein K R, Coyle S J, Hembree G G and Venables J A 1996 *J. Appl. Phys.* **80** 1161
[20] Venables J A and Harding J H 2000 *J. Cryst. Growth* **211** 27
[21] Brune H, Giovannini H, Bromann K and Kern K 1998 *Nature* **394** 451
[22] Kotrla M, Krug J and Šmilauer P 2001 *Surf. Sci.* **454–456** 681
Kotrla M, Krug J and Šmilauer P 2001 *Surf. Sci.* **482–485** 840
[23] Amaral L A N and Krug J 1997 *Phys. Rev.* E **55** 7785
Krug J 2002 *Europhys. Lett.* **60** 788
[24] Amar J G 2006 *Comput. Sci. Eng.* **8** 9
[25] Voter A F 2005 *Radiation Effects in Solids* ed K E Sickafus and E A Kotomin (Dordrecht: Springer, NATO Publishing Unit) (IPAM Publication 5898)
[26] Stangl M, Liptak M, Fletcher A, Acker J, Thomas J, Wendrock H, Oswald S and Wetzig K 2008 *Microelectron. Eng.* **85** 534
[27a] Maroutian T, Douillard L and Ernst H-J 2001 *Phys. Rev.* B **64** 165401
[27b] Néel N, Maroutian T, Douillard L and Ernst H-J 2003 *J. Phys.: Condens. Matter* **15** S3227
[28] Pierre-Louis O, D'Orsogna M R and Einstein T L 1999 *Phys. Rev. Lett.* **82** 3661
[29] Nita F and Pimpinelli A 2005 *Phys. Rev. Lett.* **95** 106104
[30] Stoyanov S and Kashiev D 1981 *Current Topics in Materials Science* ed E Kaldis (Amsterdam: North-Holland) p 69
[31] Kandel D 1997 *Phys. Rev. Lett.* **78** 499
[32] Rost M, Šmilauer P and Krug J 1996 *Surf. Sci.* **369** 393
[33] Lim J-W, Bae J W, Mimura K and Isshiki M 2005 *Japan. J. Appl. Phys.* **44** 373
[34] Sathiyanarayanan R, BH Hamouda A and Einstein T L 2008 unpublished
Sathiyanarayanan R, BH Hamouda A and Einstein T L 2008 *Materials Research Society Fall 2008 Mtg (abstract W12.2)*
[35] Thiel P 2008 private communication
[36] Mehmood F, Kara A, Rahman T S and Bohnen K P 2006 *Phys. Rev.* B **74** 155439
[37] Kandel D and Weeks J D 1994 *Phys. Rev.* B **49** 5554
Kandel D and Weeks J D 1995 *Phys. Rev.* B **52** 2154
[38] Ranganathan M and Weeks J D 2009 unpublished
[39] Tamai A, Auwärter C C W, Baumberger F, Greber T and Osterwalder J 2004 *Surf. Sci.* **566** 633
[40] Mativetsky J M, Burke S A, Fostner S and Grutter P 2007 *Small* **3** 818
[41] Xiao W, Ruffieux P, Aït-Mansour K, Groóning O, Palotas K, Hofer W A, Grooning P and Fasel R 2006 *J. Phys. Chem.* B **110** 21394
[42] Liu S, Zhang Z, Comsa G and Metiu H 1993 *Phys. Rev. Lett.* **71** 2967
[43] Stasevich T J, Gebremariam H, Einstein T L, Giesen M, Steimer C and Ibach H 2005 *Phys. Rev.* B **71** 245414
[44] Khare S V and Einstein T L 1996 *Phys. Rev.* B **54** 11752
[45] Szalma F, Gebremariam H and Einstein T L 2005 *Phys. Rev.* B **71** 035422
[46] Stasevich T J and Einstein T L 2007 *Multiscale Model. Simul.* **6** 90
[47] Mulheran P A and Blackman J A 1995 *Phil. Mag. Lett.* **72** 55
Mulheran P A and Blackman J A 1996 *Phys. Rev.* B **53** 10261
[48] Guhr T, Müller-Groeling A and Weidenmüller H A 1998 *Phys. Rep.* **299** 189
[49] Mehta M L 1991 *Random Matrices* 2nd edn (New York: Academic)
[50] For explicit details see, e.g. Zwerger W 1998 *Quantum Transport and Dissipation* ed T Dittrich *et al* (Weinheim: Wiley–VCH) chapter 1
[51] Haake F 1991 *Quantum Signatures of Chaos* (Berlin: Springer)
[52] Calogero F 1969 *J. Math. Phys.* **10** 2191
Calogero F 1969 *J. Math. Phys.* **10** 2197
Sutherland B 1971 *J. Math. Phys.* **12** 246

Sutherland B 1971 *J. Math. Phys.* **12** 251
Sutherland B 1971 *Phys. Rev.* A **4** 2019
[53] Dyson F J 1962 *J. Math. Phys.* **3** 140
Dyson F J 1962 *J. Math. Phys.* **3** 157
Dyson F J 1962 *J. Math. Phys.* **3** 166
[54] Dyson F J 1962 *J. Math. Phys.* **3** 1191
Dyson F J 1972 *J. Math. Phys.* **13** 90
[55] Narayan O and Shastry B S 1993 *Phys. Rev. Lett.* **71** 2106
[56] Einstein T L 2007 *Appl. Phys.* A **87** 375
Einstein T L 2003 *Ann. Henri Poincaré* **4** (Suppl. 2) S811
[57] Einstein T L, Richards H L, Cohen S D and Pierre-Louis O 2001 *Surf. Sci.* **493** 460
[58] Giesen M 2001 *Prog. Surf. Sci.* **68** 1
[59] Richards H L and Einstein T L 2005 *Phys. Rev.* E **72** 016124
[60] Pimpinelli A, Gebremariam H and Einstein T L 2005 *Phys. Rev. Lett.* **95** 246101
[61] BH Hamouda A, Pimpinelli Alberto and Einstein T L 2008 *Surf. Sci.* **602** 3569
[62] Pratontep S, Brinkmann M, Nüesch F and Zuppiroli L 2004 *Phys. Rev.* B **69** 165201